

Activity cycles in RS-CVn Stars

C. I. Martínez^{1,2*}, P. J. D. Mauas^{3,4†}, A. P. Buccino^{3,4}

¹Observatorio Astronómico Félix Aguilar, Universidad Nacional de San Juan, Av. Benavides 8175 oeste, CP 5400 San Juan, Argentina.

²Instituto de Ciencias Astronómicas de la Tierra y el Espacio (CONICET-UNSJ), Av. España 1512 sur, San Juan, Argentina.

³Instituto de Astronomía y Física del Espacio (CONICET-UBA), C.C. 67 Sucursal 28, C1428EHA-Buenos Aires, Argentina.

⁴Departamento de Física. Facultad de Ciencias Exactas y Naturales - Universidad de Buenos Aires, Buenos, Argentina.

12 November 2021

ABSTRACT

We compile a list of 121 RS CVn type stars from the bibliography in southern hemisphere, to search for activity cycles, covering a large range of luminosities and rotation periods. For each system of the list, we obtain photometric data from the All Sky Automated Survey (ASAS), and we complement it with our own photometry, obtained with the Optical Robotic Observatory (ORO). We analyze this data with the Generalized Lomb–Scargle periodogram to determine the rotation period and possible activity cycles for each system. We found rotation periods for 102 systems and activity cycles for 91 systems. From the statistical analysis of the results, we found that giant stars behave differently than subgiants and main-sequence stars, and that there is a good correlation between rotation periods and luminosities.

Key words: stars: activity - stars: rotation - stars: binaries: spectroscopic.

1 INTRODUCTION

RS CVn stars are close binaries where the hottest component, the *primary*, is a subgiant or giant star of spectral type between F and K, and the coolest component, the *secondary*, is a dwarf or subgiant of spectral type from G to M (Biermann & Hall 1976). The prototypical example, which gives its name to the group, is the eclipsing binary RS Canum Venaticorum. As a result of the much fainter luminosity of the coolest star, most of these systems are of the SB1 type.

These stars are fast rotators tidally synchronized, and are therefore more active than single stars with the same characteristics (Hall 1972; Dempsey et al. 1993), and they usually show strong H α , Ca II, X-ray, and microwave emissions. This activity is dominated by the hottest component, which exhibits a high rotational rate (Weiler 1978). In the optical band, the most prominent feature is the periodic photometric variability, much larger than in individual stars with the same spectral type (Dempsey et al. 1993). This variability is due to the rotational modulation by large starspots, covering almost 10% of the stellar surface (Vogt et al. 1999).

Walter et al. (1978) determined that RS CVn are also strong X-ray sources, with fluxes between 10^{26} and $10^{31.5}$ erg s $^{-1}$, and Dempsey et al. (1993) found that the temporal variations in X-rays are of the order of the starspot life-time. Singh et al. (1996) proposed that the X-ray variability is related to the tidally induced rotation

that enhances the dynamo activity, since they did not find clear evidence that it might be due to mass transference between the components.

On the other hand, many of these systems show long-term chromospheric activity variations and activity cycles (Hall et al. 1991; Berdyugina & Henry 2007; Messina 2008; Buccino & Mauas 2009; Martínez et al. 2019). To study these cycles is key to understand the connection between stellar rotation and long-term activity (see for example Rodono et al. 1986; Berdyugina et al. 1999), and it is relevant to constrain the mechanism responsible for the generation and maintenance of the stellar magnetic fields (Weiler 1978). With this goal, we have studied the long-term activity of different main-sequence stars, and we have detected cycles in many of them (Cincunegui et al. 2007; Díaz et al. 2007; Buccino et al. 2011, 2014; Flores et al. 2017; Ibañez Bustos et al. 2019a,b).

From statistical studies of activity in late-type stars with rotation periods between 22 and 48 days, Noyes et al. (1984) found a possible correlation between the activity-cycle period P_{cyc} and the Rossby number $Ro = P_{\text{rot}}/\tau_c$, where τ_c is the convective turnover time near the bottom of the convection zone.

Later, Saar & Baliunas (1992) reported that stellar activity cycles form two distinct branches when plotted as a function of the rotation period, a fact that was later confirmed by Saar & Brandenburg (1999); Böhm-Vitense (2007) and Brandenburg et al. (2017). Brandenburg et al. (1998) found that the ratio $P_{\text{cyc}}/P_{\text{rot}}$ is proportional to the α -effect in the mean field dynamo theory. Tuominen et al. (1988) found that this ratio decreases systematically with increasing thickness of the convection zone. Outside the main-

* Contact e-mail: cmartinez@conicet.gov.ar

† Contact e-mail: pablo@iafe.uba.ar

2 C. I. Martínez

sequence, evolved stars can develop increasingly thick convective envelopes and their convective turnover time increases (Gilliland 1985). Simultaneously, the rotation period of the giant stars will also increase due to rotational braking (Skumanich 1972). Therefore, studying activity cycles in evolved stars should help understand the dynamo mechanisms responsible for stellar activity.

In this work, we look for activity cycles on a large set of RS CVn-type stars, using photometric data obtained by the All Sky Automated Survey (ASAS, Pojmanski 2002), and our own photometry obtained with the Optical Robotic Observatory (ORO). In Section 2 we present our stellar list and the observations dataset. In Section 3 we describe the method used to study the temporal evolution of the data, the correlation between the stellar variables that characterize our targets and the statistical analysis. Finally, in Section 4 we discuss the results.

2 OBSERVATIONS AND DATA COLLECTION

2.1 Target list

To our knowledge, there is not available a reliable list of RS CVn-type stars in the southern hemisphere. Therefore, it is important to build a list as complete as possible of confirmed RS CVn stars. In first approach, we obtained a preliminary classification from an exhaustive search in the bibliography of bright southern stars ($V \leq 14$ and $Dec < 0$).

We first explored the southern brighter stars catalog of Bidelman & MacConnell (1973) together with the southern RS CVn candidate list of Weiler & Stencel (1979). We confirm the targets as RS CVn-type using the catalogs of active binary stars published by Rodono et al. (1986), Strassmeier et al. (1988), Pallavicini et al. (1992) and Strassmeier et al. (1993); the RS CVn binaries catalog of Morris & Mutel (1988) for radio sources and Fleming et al. (1989) for X-ray sources; and the stellar classification catalogs given by Berdnikov & Pastukhova (2008) and Drake et al. (2014). We also included all the stars individually classified by Pollard et al. (1989), Pandey et al. (2005), Strassmeier (2000), Drake (2006), Gálvez et al. (2009) and López-Santiago et al. (2012).

Finally, we added a few stars following the criteria established by Hall (1976)¹. The spectral type of the stars were obtained from the classification catalogs of Houk (1982), Stocke et al. (1991), Pourbaix et al. (2004), Torres et al. (2006) and Skiff (2014); the catalogs of chromospherically active stars by Fekel et al. (1986), Popper (1991), Randich et al. (1993), Thatcher & Robinson (1993), Fekel & Henry (2005), Bernhard et al. (2010) and Boro Saikia et al. (2018); and the of X-ray emission sources by Cutispoto et al. (1996), Kang et al. (1996), Cutispoto et al. (1999), Hüensch et al. (1999), Fuhrmeister & Schmitt (2003), Shtykovskiy & Gilfanov (2005), Haakonsen & Rutledge (2009) and Kiraga (2012).

In total, our final list, presented in Table 1, includes 121 sources.

A statistic exploratory analysis allowed us to characterize our target list and estimate the distribution of different stellar parameters, also listed in Table 1. These quantities were obtained from the next catalogs:

- The Hipparcos Catalogue (Perryman et al. 1997): V y B magnitudes, $B - V$ color index.

¹ This classification describes the main features of the RS CVn stars: spectral types between F-M with one or both evolved components, high rotation rate, chromospheric and X-ray emission.

- ASAS Photometry of ROSAT Sources (Kiraga 2012): V magnitude.
- The Tycho-2 catalogue (Hög et al. 2000): V and B magnitudes, $B - V$ color index.
- The International Variable Star Index (Watson et al. 2006): rotation periods.
- The PASTEL catalogue, 2016 version (Soubiran et al. 2016): effective temperature T_{eff} .
- Gaia Data Release 2 (Gaia Collaboration 2018): G (330-1050 nm), G_{BP} (330-680 nm) and G_{RP} (630-1050 nm) apparent magnitudes, T_{eff} and luminosity $\log L$.

In Fig. 1 we show the histograms for the colours $B - V$ and $G_{BP} - G_{RP}$, the effective temperature T_{eff} and the luminosity $\log L$. In each graph N is the number of sources for which the specific quantity was available.

2.2 Observations

We used photometric data provided by the ASAS-3 database, which is available for our 121 stars. We only used observations qualified as A or B in the database (*best* or *mean* quality according to the ASAS definition).

We also carried out photometric observations from February 2017 to January 2019 using the three 16" MEADE telescopes that are part of the Optical Robotic Observatory (ORO) installed at the Estación en Altura Carlos U. Cesco, located in San Juan, Argentina. We observed 8-10 objects per night in non-consecutive nights to have a nearly uniform sample throughout their expected rotation periods. The image calibration and aperture differential photometry were optimally performed using our package *killastro*, developed under the IRAF² platform. This package tries 10 different apertures, ranging from 0.7 to 4 FWHM, and chooses the aperture which minimizes the flux dispersion. We then performed differential photometry on these images, using as reference stars between 2 and 4 stars which do not show variability in the ASAS database. Finally, we intercalibrate with ASAS using the ASAS magnitude of the brightest reference star in the field (for details, see Martínez et al. 2019).

3 ACTIVITY CYCLES ANALYSIS

The Lomb–Scargle (LS) periodogram (Horne & Baliunas 1986) has been widely used to search for stellar activity cycles. Zechmeister & Kürster (2009) proposed a modification which has certain advantages in comparison to the classic LS periodogram: the Generalized Lomb–Scargle (GLS) periodogram. Namely, it takes into account a varying zero point, it does not require bootstrap or Monte Carlo algorithms to compute the significance of a signal, reducing the computational cost, and it is less susceptible to aliasing than the LS periodogram. In this study, we used the Python libraries developed by Czesla et al. (2019).

First, we applied to the light curves of all the sources the GLS periodogram in the 0.1 to 150 days range, to determine the rotation period of each target. This range was selected according to the maximum and minimum orbital periods of RS CVn-type systems found by Strassmeier et al. (1993). However, we usually found weak peaks that could not be distinguished from noise, or with high levels

² The Image Reduction and Analysis Facility (IRAF) is distributed by the Association of Universities for Research in Astronomy (AURA), Inc., under contract to the National Science Foundation

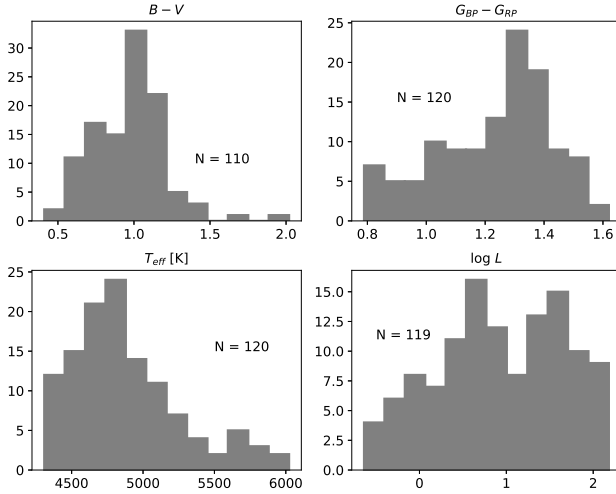


Figure 1. Distribution of the stellar parameters in our list. The shaded region shows the results for the whole sample, and the coloured lines the clustering groups described in Sect. 3

of FAP. In fact, the photometric modulation attributed to rotation is usually not persistent throughout the entire data set. The absence of a well-defined photometric modulation at different epochs could be the result of longitudinal distributions of spots which are more or less homogeneous (Murdoch et al. 1995). Therefore, we looked in the periodogram for long-term variations associated with possible activity cycles, choosing periods longer than 150 days, and we obtained significant periods for 91 stars.

Then, we fitted the light curves with a sinusoidal function for the period found, we applied the GLS to the residuals for the period range between 0.1 and 150 days, and we found rotation periods for 102 sources. In several cases, marked with a \star in Table 1, we found that the amplitude of the rotational modulation changes during the activity cycle, due to the different filling factor of spots and active regions.

We complemented this analysis with periods for 13 sources found in *The International Variable Star Index* (VSX, Watson et al. 2006). For the eclipsing binaries, indicated with a \dagger in Table 1, we used the phase dispersion minimization algorithm (PDM, Stellingwerf 1978) provided in IRAF, and we list the orbital period instead. All the periods obtained are listed in Table 1, and the phase curves are shown in Figure 6. It can be seen in this figure that in a few cases the phase coverage of the observations is not adequate. We plan to complete the coverage with future observations.

We also applied to the data set the hierarchical agglomerative clustering with Ward linkage and Euclidean distance described by Ward (1963), considering the variables P_{rot} , P_{cyc} , A_{cyc} , T_{eff} and $\log L$. In fact, we found that the sample can be separated in two different clusters. In Fig. 2 we show our stars in the HR diagram, with both clusters indicated with different colours. It can be seen that the stars marked in blue are giant stars, while those marked in red are closer to the main-sequence.

In Fig. 3 we show the distribution of our results for the whole sample and for both clusters. We plot P_{rot} , P_{cyc} and the activity cycle amplitude A_{cyc} , expressed as percentage of the mean magnitude V (% mmag). It can be seen that the red group has shorter rotation periods and cycles both longer and with larger amplitudes. This last result can also be seen in Fig. 4, where we plot the activity period P_{cyc} as a function of the rotation period P_{rot} for each agglomerate.

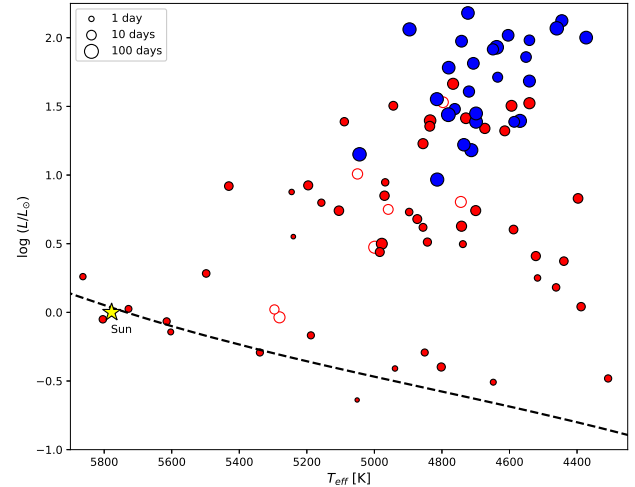


Figure 2. HR diagram: Luminosity vs. effective temperature. The clustering we found is shown in red and blue. The size of each point is proportional to the rotation period. The theoretical main-sequence is represented by a black dotted line.

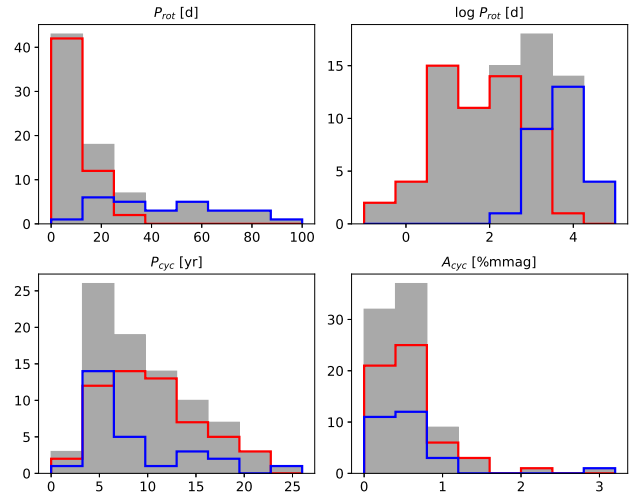


Figure 3. Distribution of the GLS results: P_{rot} in two different scales, P_{cyc} and its amplitude A_{cyc} . The shaded regions show the results for the whole sample, and the coloured lines represent the clustering groups; there are 56 objects in cluster 1 (red) and 27 objects in cluster 2 (blue).

For the cluster #2 (blue color), associated to giant stars, we found that $P_{\text{cyc}}/P_{\text{rot}} = 75 \pm 38$ and $\log(P_{\text{cyc}}/P_{\text{rot}}) = 1.81 \pm 0.26$. For comparison, Böhm-Vitense (2007), in a study of main-sequence stars, obtained $\log(P_{\text{cyc}}/P_{\text{rot}}) = 1.95$ for the *inactive* branch.

Finally, to look for correlations between the stellar properties in our target list, we used the non-parametrical Spearman correlation coefficient r_{ij} (Conover 1999), which can be applied to variables with non-Gaussian distributions. The quantities we analyzed form a variable vector \mathbf{v} , given by:

$$\mathbf{v} = [P_{\text{rot}} \quad P_{\text{cyc}} \quad A_{\text{cyc}} \quad T_{\text{eff}} \quad \log L], \quad (1)$$

and the results can be summarized by a matrix \mathbf{R} . In this matrix, the elements r_{ij} below the main diagonal represent the correlation between the i -th y j -th variables, and the elements p_{ij} above the main

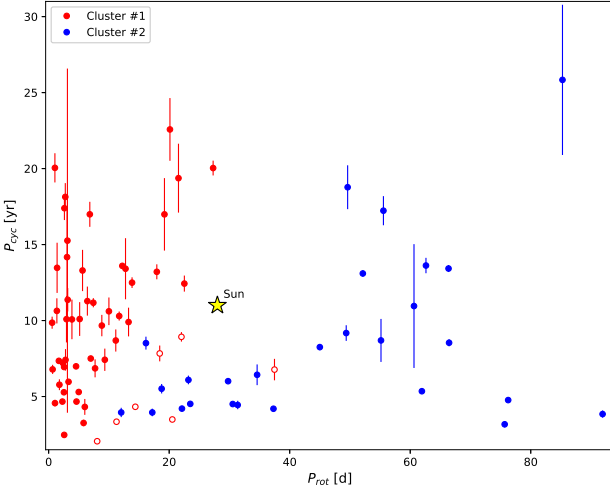


Figure 4. Rotation vs. activity periods. The two groups found in the clustering are shown in red and blue. The position of the Sun is indicated by the yellow star.

diagonal represent the probability that the i -th and j -th variables are independent.

The r_{ij} coefficients indicate if the correlation is perfect ($|1|$), excellent ($|0.9 - 1|$), acceptable ($|0.75 - 0.9|$), regular ($|0.5 - 0.75|$), weak ($|0.25 - 0.5|$) or absent (< 0.25). r_{ij} is positive for a direct correlation and negative for an inverse one.

The result we obtained is:

$$\mathbf{R} = \begin{bmatrix} 1 & 0.64 & 0.1 & * & * \\ -0.05 & 1 & * & 0.51 & 0.59 \\ 0.18 & 0.63 & 1 & 0.01 & 0.83 \\ -0.36 & -0.07 & -0.26 & 1 & * \\ 0.76 & -0.06 & 0.02 & -0.35 & 1 \end{bmatrix}. \quad (2)$$

The matrix elements pointed out with a * represent probability values lower than 0.0005. From these results, it seems that there is a good positive correlation between rotation period P_{rot} and luminosity $\log L$, and a regular correlation between the activity period P_{cyc} and its amplitude A_{cyc} .

We therefore plot the rotation periods P_{rot} in logarithmic scale as a function of the luminosity L/L_{\odot} in Fig. 5. The correlation found in (2), with $R_s = 0.76$, is apparent. The two groups seen in Fig. 2 are separated by luminosity. Fitting this correlation, we obtain that:

$$P_{\text{rot}} \approx 3.16 \left(\frac{L}{L_{\odot}} \right)^{3/5}. \quad (3)$$

4 CONCLUSIONS

In this work we present a list of 121 bona fide RS CVn southern stars with $V \leq 14$. For this list, we compiled the main stellar parameters: the colour index $B - V$, the effective temperature T_{eff} and the luminosity L (see 1)

We also analyzed the activity of these systems in different time scales. Applying the Generalized Lomb-Scargle periodogram (GLS) to photometric data obtained from the publicly available ASAS-3 database and our own observations obtained with ORO, we found rotation periods for 102 systems, which we completed with results from the literature for 13 more. We also obtained activity

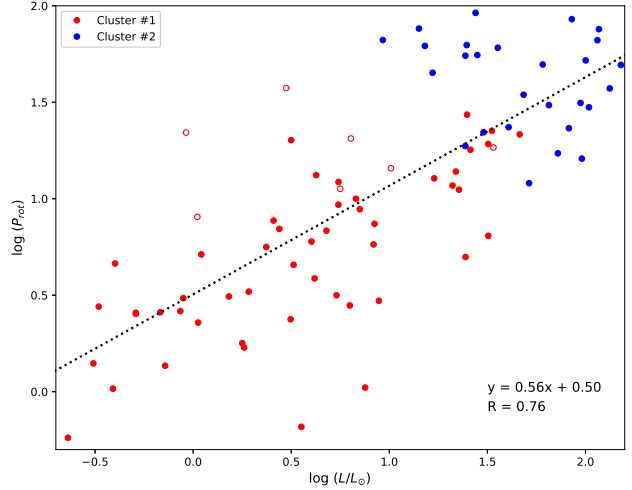


Figure 5. $\log(P_{\text{rot}})$ versus $\log(L/L_{\odot})$. The clustering is shown with the same colour code than in the other figures. The R -spearman coefficient for this correlation is 0.76.

cycles for 91 systems. In many cases, we observed that the amplitude variation due to the rotation is modulated by the activity cycle, due to the different area covered by starspots.

We applied a hierarchical agglomerative clustering method to our data and found that giant stars are separated from subgiants and main-sequence stars.

We also found a good correlation between the rotation period P_{rot} and the luminosity $\log L$, and a fair one between the activity period P_{cyc} and the percent amplitude variation A_{cyc} .

5 ACKNOWLEDGMENTS

We are grateful to the personal of the Observatorio Astronómico Félix Aguilar for their invaluable help with the operation of the Optical Robotic Observatory.

6 DATA AVAILABILITY

The data underlying this article will be shared on reasonable request to the corresponding author.

REFERENCES

- Berdnikov L. N., Pastukhova E. N., 2008, Peremennye Zvezdy, **28**, 9
- Berdyugina S. V., Henry G. W., 2007, *ApJ*, **659**, L157
- Berdyugina S. V., Berdyugin A. V., Ilyin I., Tuominen I., 1999, *A&A*, **350**, 626
- Bernhard K., Lloyd C., Frank P., 2010, Berliner Arbeitsgemeinschaft fuer Veraenderliche Sterne - Mitteilungen, **210**, 1
- Bidelman W. P., MacConnell D. J., 1973, *AJ*, **78**, 687
- Biermann P., Hall D. S., 1976, in Eggleton P., Mitton S., Whelan J., eds, IAU Symposium Vol. 73, Structure and Evolution of Close Binary Systems. p. 381
- Böhm-Vitense E., 2007, *ApJ*, **657**, 486
- Boro Saikia S., et al., 2018, *A&A*, **616**, A108
- Brandenburg A., Saar S. H., Turpin C. R., 1998, *ApJ*, **498**, L51
- Brandenburg A., Mathur S., Metcalfe T. S., 2017, *ApJ*, **845**, 79
- Buccino A. P., Maunas P. J. D., 2009, *A&A*, **495**, 287

- Buccino A. P., Díaz R. F., Luoni M. L., Abrevaya X. C., Mauas P. J. D., 2011, [AJ](#), **141**, 34
- Buccino A. P., Petracci R., Jofré E., Mauas P. J. D., 2014, [ApJ](#), **781**, L9
- Circunegui C., Díaz R. F., Mauas P. J. D., 2007, [A&A](#), **461**, 1107
- Conover W. J., 1999, Practical Nonparametric Statistics. Ed. John Wiley & Sons, Inc.
- Cutispoto G., Tagliaferri G., Pallavicini R., Pasquini L., Rodono M., 1996, [A&AS](#), **115**, 41
- Cutispoto G., Pastori L., Tagliaferri G., Messina S., Pallavicini R., 1999, [A&AS](#), **138**, 87
- Czesla S., Schröter S., Schneider C. P., Huber K. F., Pfeifer F., Andreasen D. T., Zechmeister M., 2019, PyA: Python astronomy-related packages (ascl:1906.010)
- Dempsey R. C., Linsky J. L., Fleming T. A., Schmitt J. H. M. M., 1993, [ApJS](#), **86**, 599
- Díaz R. F., González J. F., Circunegui C., Mauas P. J. D., 2007, [A&A](#), **474**, 345
- Drake A. J., 2006, [The Astronomical Journal](#), **131**, 1044
- Drake A. J., et al., 2014, [ApJS](#), **213**, 9
- Fekel F. C., Henry G. W., 2005, [AJ](#), **129**, 1669
- Fekel F. C., Moffett T. J., Henry G. W., 1986, [ApJS](#), **60**, 551
- Fleming T. A., Gioia I. M., Maccacaro T., 1989, [AJ](#), **98**, 692
- Flores M. G., Buccino A. P., Saffe C. E., Mauas P. J. D., 2017, [MNRAS](#), **464**, 4299
- Führmeister B., Schmitt J. H. M. M., 2003, [A&A](#), **403**, 247
- Gaia Collaboration 2018, [A&A](#), **616**, A1
- Gálvez M. C., Montes D., Fernández-Figueroa M. J., De Castro E., Cornide M., 2009, [AJ](#), **137**, 3965
- Gilliland R. L., 1985, [ApJ](#), **299**, 286
- Haakonsen C. B., Rutledge R. E., 2009, [ApJS](#), **184**, 138
- Hall D. S., 1972, [PASP](#), **84**, 323
- Hall D. S., 1976, Astrophysics and Space Science Library, **60**, 287
- Hall D. S., et al., 1991, [J. Astrophys. Astron.](#), **12**, 281
- Høg E., et al., 2000, [A&A](#), **355**, L27
- Horne J. H., Baliunas S. L., 1986, [ApJ](#), **302**, 757
- Houk N., 1982, Michigan Catalogue of Two-dimensional Spectral Types for the HD stars. Volume 3. Declinations -40 to -26. Department of Astronomy, University of Michigan
- Hünsch M., Schmitt J. H. M. M., Sterzik M. F., Voges W., 1999, [A&AS](#), **135**, 319
- Ibáñez Bustos R. V., Buccino A. P., Flores M., Martínez C. I., Maizel D., Messina S., Mauas P. J. D., 2019a, [MNRAS](#), **483**, 1159
- Ibáñez Bustos R. V., Buccino A. P., Flores M., Mauas P. J. D., 2019b, [A&A](#), **628**, L1
- Kang Y. W., Guinan E. F., Guedel M., Margheim S., 1996, in American Astronomical Society Meeting Abstracts. p. 44.14
- Kiraga M., 2012, [Acta Astron.](#), **62**, 67
- López-Santiago J., Stelzer B., Saxton R., 2012, [PASP](#), **124**, 682
- Martínez C. I., González J. F., Buccino A., Ibáñez Bustos R., Mauas P. J. D., 2019, [MNRAS](#), **490**, 5832
- Messina S., 2008, [A&A](#), **480**, 495
- Morris D. H., Mutel R. L., 1988, [AJ](#), **95**, 204
- Murdoch K. A., Hearnshaw J. B., Kilmartin P. M., Gilmore A. C., 1995, [MNRAS](#), **276**, 836
- Noyes R. W., Weiss N. O., Vaughan A. H., 1984, [ApJ](#), **287**, 769
- Pallavicini R., Randich S., Giampapa M. S., 1992, [A&A](#), **253**, 185
- Pandey J. C., Singh K. P., Sagar R., Drake S. A., 2005, Bulletin of the Astronomical Society of India, **33**, 373
- Perryman M. A. C., et al., 1997, [A&A](#), **300**, 501
- Pojmanski G., 2002, [Acta Astronom.](#), **52**, 397
- Pollard K. R., Hearnshaw J. B., Gilmore A. C., Kilmartin P. M., 1989, [J. Astrophys. Astron.](#), **10**, 139
- Popper D. M., 1991, [AJ](#), **101**, 220
- Pourbaix D., et al., 2004, [A&A](#), **424**, 727
- Randich S., Gratton R., Pallavicini R., 1993, [A&A](#), **273**, 194
- Rodono M., et al., 1986, [A&A](#), **165**, 135
- Saar S. H., Baliunas S. L., 1992, in Harvey K. L., ed., Astronomical Society of the Pacific Conference Series Vol. 27, The Solar Cycle. pp 150–167
- Saar S. H., Brandenburg A., 1999, [ApJ](#), **524**, 295
- Shtykovskiy P., Gilfanov M., 2005, [A&A](#), **431**, 597
- Singh K. P., Drake S. A., White N. E., 1996, [AJ](#), **111**, 2415
- Skiff B. A., 2014, VizieR Online Data Catalog
- Skumanich A., 1972, [ApJ](#), **171**, 565
- Soubiran C., Le Campion J.-F., Brouillet N., Chemin L., 2016, [A&A](#), **591**, A118
- Stellingwerf R. F., 1978, [ApJ](#), **224**, 953
- Stocke J. T., Morris S. L., Gioia I. M., Maccacaro T., Schild R., Wolter A., Fleming T. A., Henry J. P., 1991, [ApJS](#), **76**, 813
- Strassmeier K. G., 2000, [A&A](#), **357**, 608
- Strassmeier K. G., Hall D. S., Zeilik M., Nelson E., Eker Z., Fekel F. C., 1988, [ApJS](#), **72**, 291
- Strassmeier K. G., Hall D. S., Fekel F. C., Scheck M., 1993, [A&AS](#), **100**, 173
- Thatcher J. D., Robinson R. D., 1993, [MNRAS](#), **262**, 1
- Torres C. A. O., Quast G. R., da Silva L., de La Reza R., Melo C. H. F., Sterzik M., 2006, [A&A](#), **460**, 695
- Tuominen I., Rüdiger G., Brandenburg A., 1988, Observational Constraints for Solar-Type Dynamos. D. Reidel Publishing Company, p. 13
- Vogt S. S., Hatzes A. P., Misch A. A., Kürster M., 1999, [ApJS](#), **121**, 547
- Walter F., Charles P., Bowyer S., 1978, [ApJ](#), **225**, L119
- Ward J. H., 1963, American Statistical Association, **58**, 236
- Watson C. L., Henden A. A., Price A., 2006, Society for Astronomical Sciences Annual Symposium, **25**, 47
- Weiler E. J., 1978, [MNRAS](#), **182**, 77
- Weiler E. J., Stencel R. E., 1979, [AJ](#), **84**, 1372
- Zechmeister M., Kürster M., 2009, [A&A](#), **496**, 577

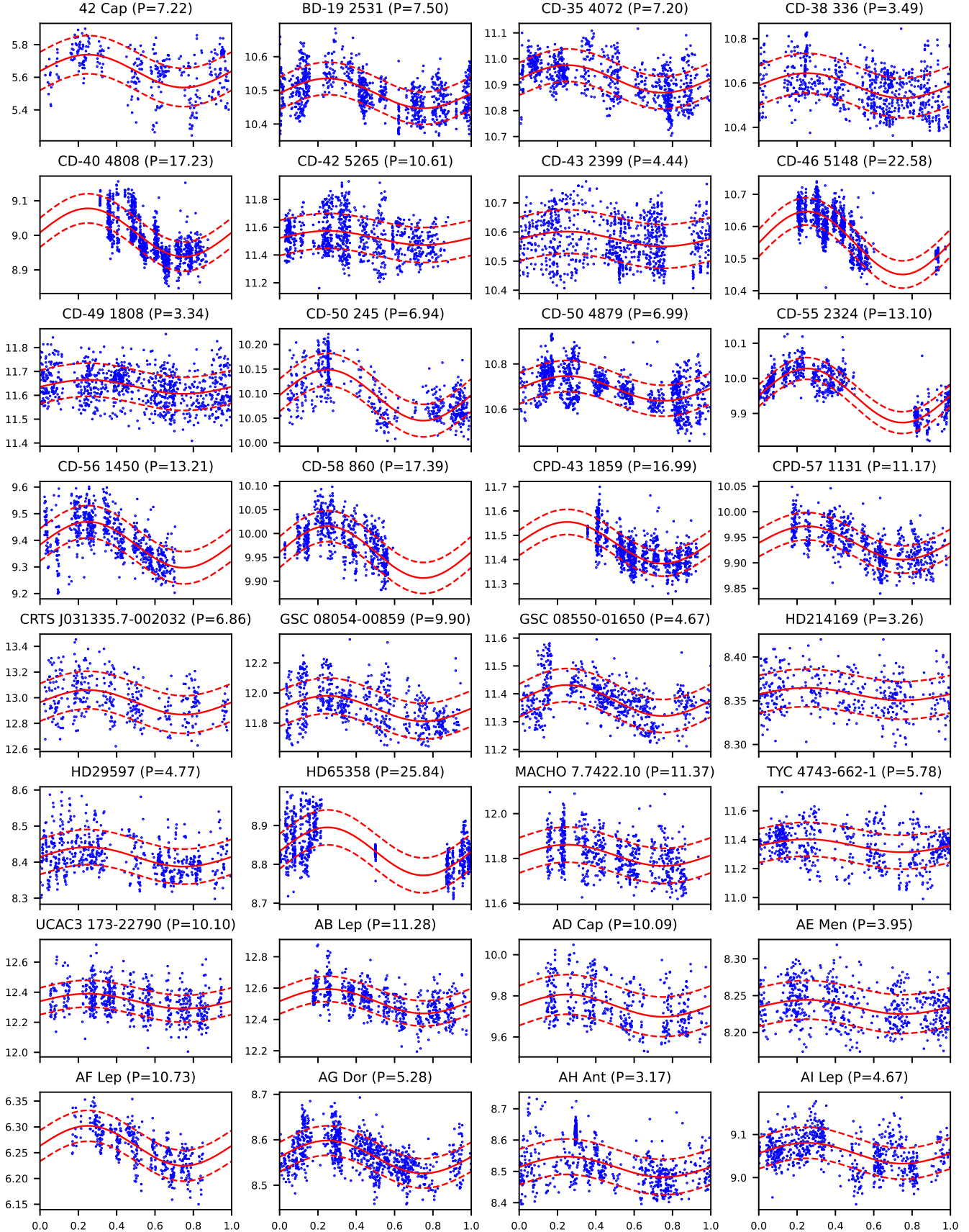
Figure 6. Phase curves for the activity cycles we detected (P is expressed in years).

Figure 6. (continued)

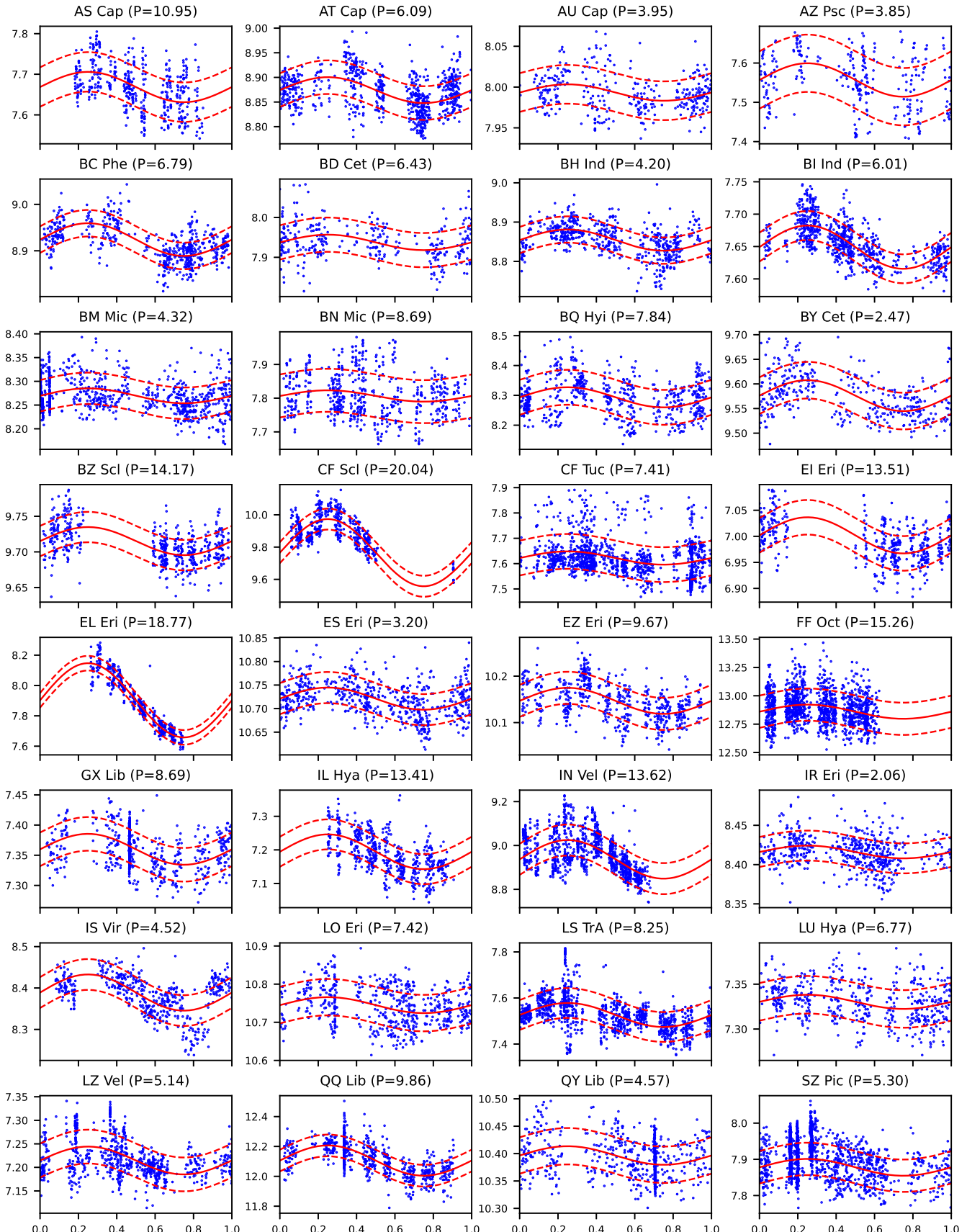


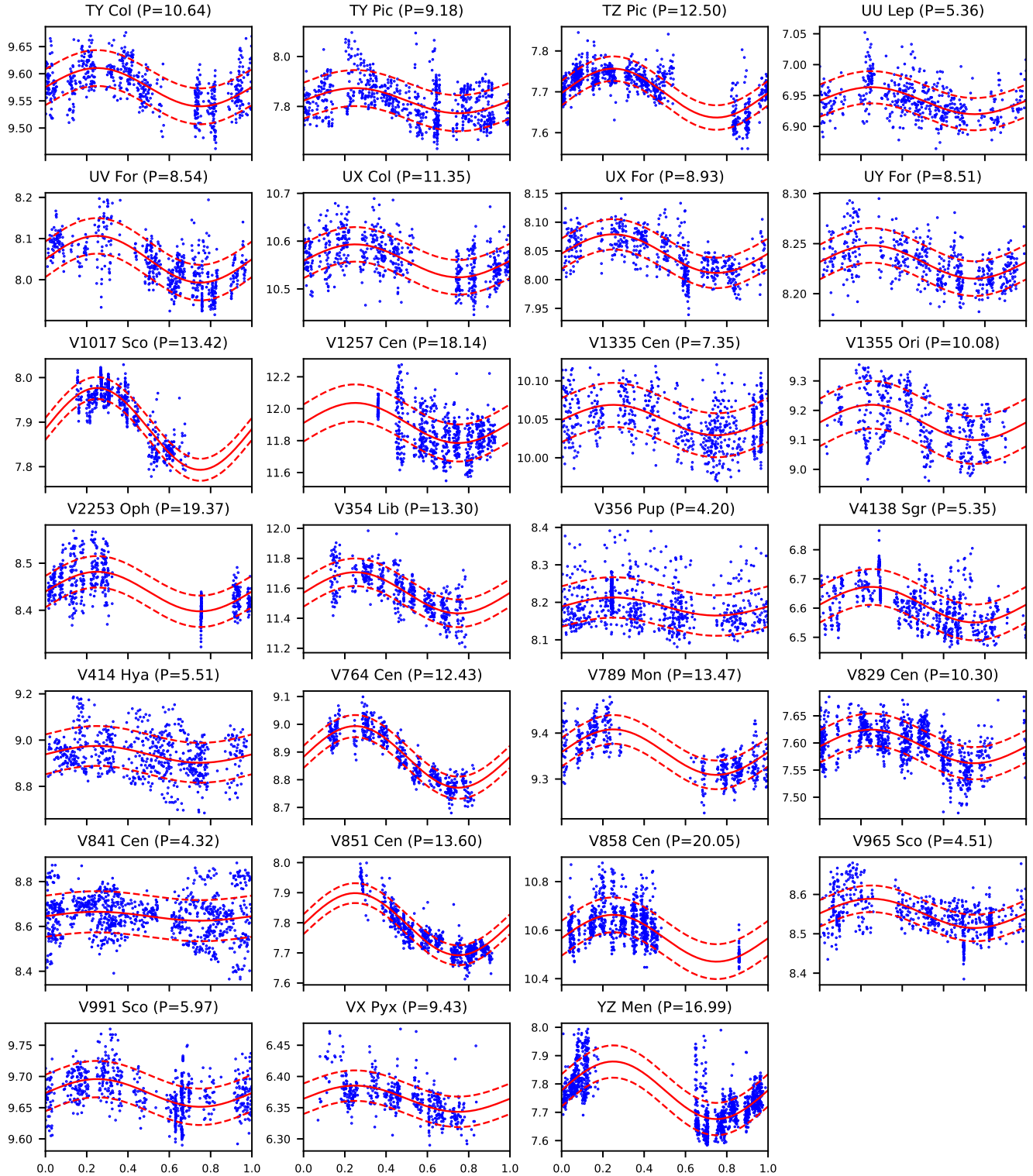
Figure 6. (continued).

Table 1. The complete list of our targets, including our results. The different columns list (from left to right) the star ID, the V magnitude, the $B - V$ colour index, the effective temperature of the binary system, the luminosity in logarithm scale, the short-period associated to the stellar rotation, the error in the short-period determination, the FAP corresponding to the short-period, the long-period associated to the stellar activity cycle, the long-period amplitude, the error in the long-period determination and the FAP corresponding to the long-period. \ddagger rotation period obtained from *The International Variable Star Index* (VSX). \star stars having a rotation amplitude which varies during the activity cycle. \dagger eclipsing binaries.

ID	V	$B - V$	T_{eff} [K]	$\log L$ [L_{\odot}]	P_{rot} [d]	FAP (P_{rot})	P_{cyc} [yr]	A_{cyc} [%]	FAP (P_{cyc})
*42 Cap	5.18	0.65	5682	0.99	-	-	7.22 ± 2.39	1.79	10^{-4}
*del Eri	3.54	0.92	5023	0.60	-	-	-	-	-
1E2157.6-1016	12.54	-	4395	0.36	7.108 ± 0.001	-	-	-	-
BD-19 2531	10.51	0.69	4984	0.44	6.984 ± 0.001	$< 10^{-15}$	7.50 ± 0.16	0.42	$< 10^{-15}$
CD-35 4072	10.93	0.83	4738	0.50	2.373 ± 0.0001	$< 10^{-15}$	7.20 ± 0.18	0.49	$< 10^{-15}$
CD-38 336 \star	10.59	1.26	4744	0.80	20.521 ± 0.006	$< 10^{-15}$	3.49 ± 0.03	0.53	$< 10^{-15}$
CD-40 4808 \star	9.00	1.13	4699	1.45	55.552 ± 0.055	$< 10^{-15}$	17.23 ± 0.96	0.77	$< 10^{-15}$
CD-42 130	10.55	1.68	4989	0.72	16.941 ± 0.007	-	-	-	-
CD-42 5265 \star	11.44	1.16	4397	0.83	9.998 ± 0.002	$< 10^{-15}$	10.61 ± 0.91	0.44	$< 10^{-15}$
CD-43 2399 \star	10.58	0.83	4742	1.97	31.369 ± 0.007	$< 10^{-15}$	4.44 ± 0.28	0.24	0.08
CD-46 5148	10.40	0.93	4978	0.50	20.127 ± 0.006	$< 10^{-15}$	22.58 ± 2.06	0.93	10^{-14}
CD-49 1808	11.67	1.09	4959	0.75	11.259 ± 0.002	$< 10^{-15}$	3.34 ± 0.07	0.25	$< 10^{-15}$
CD-50 245	10.11	0.77	5339	-0.30	2.566 ± 0.0002	$< 10^{-15}$	6.94 ± 0.08	0.51	$< 10^{-15}$
CD-50 2604	9.74	0.63	5336	1.70	24.289 ± 0.011	-	-	-	-
CD-50 4879 \star	10.94	0.98	4843	0.51	4.547 ± 0.0003	$< 10^{-15}$	6.99 ± 0.14	0.51	$< 10^{-15}$
CD-55 2324	10.00	2.02	4373	2.00	52.133 ± 0.050	$< 10^{-15}$	13.10 ± 0.20	0.78	$< 10^{-15}$
CD-56 1450 \star	9.55	0.97	4729	1.41	17.948 ± 0.019	10^{-7}	13.21 ± 0.49	0.92	$< 10^{-15}$
CD-58 860	10.01	0.80	5615	-0.07	2.615 ± 0.0002	$< 10^{-15}$	17.39 ± 0.78	0.55	$< 10^{-15}$
CPD-43 1859	11.45	0.98	4873	0.68	6.830 ± 0.001	$< 10^{-15}$	16.99 ± 0.82	0.75	$< 10^{-15}$
CPD-57 1131	9.95	0.75	5196	0.92	7.414 ± 0.001	$< 10^{-15}$	11.17 ± 0.30	0.33	$< 10^{-15}$
CRTS J031335.7-002032	12.70	-	4522	0.41	7.704 ± 0.001	$< 10^{-15}$	6.86 ± 0.59	0.74	10^{-6}
CRTS J205535.2-153510	12.88	-	4760	1.08	10.650 ± 0.004	-	-	-	-
CRTS J225004.4-075247	13.16	-	4897	0.96	42.112 ± 0.054	-	-	-	-
GSC 08054-00859 \star	11.71	1.09	4742	0.63	13.257 ± 0.002	$< 10^{-15}$	9.90 ± 0.94	0.71	10^{-10}
GSC 08550-01650	11.43	0.90	4802	-0.39	4.618 ± 0.001	10^{-9}	4.67 ± 0.10	0.49	$< 10^{-15}$
Haro 5-72	13.86	-	4310	-0.25	5.929 ± 0.002	-	-	-	-
HD 214169	8.38	0.96	5431	0.92	5.796 ± 0.001	10^{-9}	3.26 ± 0.21	0.09	0.001
HD 29597 \star	8.40	0.82	5044	1.15	76.253 ± 0.084	$< 10^{-15}$	4.77 ± 0.15	0.32	$< 10^{-15}$
HD 65358 \star	8.85	1.40	4638	1.93	85.266 ± 0.139	$< 10^{-15}$	25.84 ± 4.94	0.70	$< 10^{-15}$
HD 155555	6.72	0.78	5129	0.28	1.687 ± 0.0002	-	-	-	-
HD 17925	6.05	0.86	5235	-0.39	6.710	-	-	-	-
MACHO 7.7422.10	11.88	-	4897	0.73	3.161 ± 0.0001	$< 10^{-15}$	11.37 ± 0.77	0.40	$< 10^{-15}$
TYC 4743-662-1 \star	11.25	1.44	4517	0.25	1.784 ± 0.00004	$< 10^{-15}$	5.78 ± 0.36	0.40	10^{-8}
TYC 8380-1953-1	10.45	1.06	4517	1.21	3.076 ± 0.0002	-	-	-	-
UCAC3 173-22790	12.80	-	4388	0.04	5.144 ± 0.0005	$< 10^{-15}$	10.10 ± 1.11	0.41	10^{-8}
V* AB Lep	-	-	4944	1.50	6.425 ± 0.001	10^{-13}	11.28 ± 0.95	0.62	$< 10^{-15}$
V* AD Cap \ddagger	9.77	1.00	4968	0.95	2.959 ± 0.089	-	10.09 ± 1.53	0.56	10^{-15}
V* AE Men	8.26	1.11	4635	1.71	12.038 ± 0.002	$< 10^{-15}$	3.95 ± 0.31	0.12	0.001
V* AF Lep \dagger	6.30	0.54	6496	0.25	1.000	-	10.73 ± 0.60	0.62	$< 10^{-15}$
V* AG Dor \star	8.60	0.90	4851	-0.29	2.534 ± 0.0001	$< 10^{-15}$	5.28 ± 0.09	0.42	$< 10^{-15}$
V* AH Ant	8.40	1.20	4460	2.07	75.671 ± 0.104	$< 10^{-15}$	3.17 ± 0.20	0.38	0.2
V* AI Lep	8.95	0.63	5728	0.03	2.281 ± 0.0002	10^{-7}	4.67 ± 0.12	0.27	$< 10^{-15}$
V* AK Vol	8.60	0.99	4739	1.83	31.792 ± 0.017	-	-	-	-
V* AR Mon \dagger	8.79	1.05	4709	1.84	21.211	-	-	-	-
V* AS Cap \star	7.69	1.06	4815	1.55	60.625 ± 0.050	$< 10^{-15}$	10.95 ± 4.07	0.49	0.02
V* AT Cap \ddagger	8.87	1.28	4649	1.92	23.193	-	6.09 ± 0.29	0.30	$< 10^{-15}$
V* AU Cap	8.01	1.21	4551	1.86	17.196 ± 0.012	10^{-12}	3.95 ± 0.25	0.13	10^{-5}
V* AZ Psc \star	-	-	4781	1.44	91.920 ± 0.221	$< 10^{-15}$	3.85 ± 0.24	0.56	0.01
V* BC Phe \dagger	8.92	0.71	5240	0.55	0.657	-	6.79 ± 0.30	0.39	$< 10^{-15}$
V* BD Cet \star	7.98	1.11	4541	1.68	34.593 ± 0.026	10^{-14}	6.43 ± 0.68	0.24	10^{-6}
V* BH Ind	9.12	1.04	4762	1.48	22.117 ± 0.020	10^{-7}	4.20 ± 0.09	0.30	$< 10^{-15}$

Table 1. (continued)

ID	V	B – V	T_{eff} [K]	$\log L$ [L_{\odot}]	P_{rot} [d]	FAP (P_{rot})	P_{cyc} [yr]	A_{cyc} [%]	FAP (P_{cyc})
V* BH Vir †	9.68	0.61	5876	0.43	0.817	-	-	-	-
V* BI Ind	7.67	1.22	4604	2.02	29.775 ± 0.017	$< 10^{-15}$	6.01 ± 0.10	0.44	$< 10^{-15}$
V* BM Mic ★	8.29	0.77	5050	1.01	14.382 ± 0.007	$< 10^{-15}$	4.32 ± 0.08	0.19	$< 10^{-15}$
V* BN Mic	7.76	1.11	4699	1.39	55.149 ± 0.047	$< 10^{-15}$	8.69 ± 1.42	0.22	10^{-4}
V* BQ Hyi	9.12	0.72	4797	1.53	18.430 ± 0.005	$< 10^{-15}$	7.84 ± 0.52	0.41	$< 10^{-15}$
V* BY Cet ★	9.60	0.77	5188	-0.17	2.580 ± 0.0002	10^{-12}	2.47 ± 0.05	0.33	$< 10^{-15}$
V* BZ Scl	9.68	0.64	5804	-0.05	3.053 ± 0.0002	10^{-14}	14.17 ± 3.16	0.20	$< 10^{-15}$
V* CF Oct	7.93	1.07	4881	1.62	20.376 ± 0.010	-	-	-	-
V* CF Scl	9.93	0.70	4835	1.40	27.292 ± 0.012	$< 10^{-15}$	20.04 ± 0.49	2.13	$< 10^{-15}$
V* CF Tuc ✕ †	7.90	0.41	5157	0.80	2.798	-	7.41 ± 0.71	0.34	$< 10^{-15}$
V* EI Eri	7.04	0.67	5513	0.59	-	-	13.51 ± 4.31	0.50	$< 10^{-15}$
V* EL Eri ★	8.19	1.10	4780	1.78	49.614 ± 0.065	10^{-15}	18.77 ± 1.44	3.09	$< 10^{-15}$
V* ER Eri	9.85	1.10	4666	0.69	5.920 ± 0.001	-	-	-	-
V* ES Eri	10.63	0.98	5078	-0.18	-	-	3.20 ± 0.06	0.22	$< 10^{-15}$
V* EZ Eri	10.17	1.03	4970	0.85	8.824 ± 0.001	$< 10^{-15}$	9.67 ± 0.70	0.28	$< 10^{-15}$
V* FF Oct	-	4462	0.18	3.114 ± 0.0002	$< 10^{-15}$	15.26 ± 11.32	0.49	10^{-5}	
V* GX Lib	7.35	1.04	4836	1.36	11.139 ± 0.001	$< 10^{-15}$	8.69 ± 0.73	0.35	$< 10^{-15}$
V* HU Vir	8.71	0.98	4517	0.74	10.438 ± 0.002	-	-	-	-
V* IL Hya ★	7.37	1.01	4856	1.23	12.755 ± 0.003	$< 10^{-15}$	13.41 ± 2.01	0.72	$< 10^{-15}$
V* IN Vel ★	9.08	1.18	4569	1.39	62.611 ± 0.068	$< 10^{-15}$	13.62 ± 0.51	0.99	$< 10^{-15}$
V* IN Vir	9.13	1.20	4436	0.75	8.129 ± 0.001	-	-	-	-
V* IR Eri †	8.45	0.85	5296	0.02	8.050	-	2.06 ± 0.05	0.10	10^{-8}
V* IS Vir †	8.43	1.07	4720	1.61	23.500	-	4.52 ± 0.10	0.52	$< 10^{-15}$
V* LO Eri ★	10.76	0.89	5105	0.74	9.318 ± 0.001	$< 10^{-15}$	7.42 ± 0.73	0.19	10^{-10}
V* LS TrA ★	8.14	1.04	4735	1.22	44.997 ± 0.041	$< 10^{-15}$	8.25 ± 0.20	0.69	$< 10^{-15}$
V* LU Hya	7.35	0.95	4999	0.47	37.474 ± 0.050	10^{-10}	6.77 ± 0.71	0.11	10^{-6}
V* LZ Vel ★	7.19	1.27	4420	3.39	92.791 ± 0.306	$< 10^{-15}$	5.14 ± 0.05	0.41	$< 10^{-15}$
V* NR Lib	11.34	0.93	4571	0.30	2.683 ± 0.0001	-	-	-	-
V* QQ Lib †	11.89	0.56	5051	-0.64	0.577	-	9.86 ± 0.40	0.84	$< 10^{-15}$
V* QY Lib	10.41	0.81	5245	0.88	1.050 ± 0.00002	$< 10^{-15}$	4.57 ± 0.21	0.16	$< 10^{-15}$
V* RV Lib †	9.17	1.09	4708	1.41	10.721	-	-	-	-
V* RZ Eri †	7.88	0.65	5324	1.49	39.282	-	-	-	-
V* SZ Pic	7.91	0.75	5089	1.39	4.988 ± 0.001	$< 10^{-15}$	5.30 ± 0.17	0.30	10^{-4}
V* TW Lep	7.47	1.05	4805	1.71	27.752 ± 0.025	-	-	-	-
V* TX Pic	6.10	1.16	4559	2.13	20.914 ± 0.033	-	-	-	-
V* TY Col	9.60	0.68	5603	-0.14	1.363 ± 0.0001	10^{-6}	10.64 ± 0.83	0.37	$< 10^{-15}$
V* TY Pic ★	7.70	0.99	4723	2.18	49.378 ± 0.037	$< 10^{-15}$	9.18 ± 0.51	0.65	$< 10^{-15}$
V* TY Pyx †	6.87	0.69	5669	0.67	3.199	-	-	-	-
V* TZ Col	9.08	0.59	5907	0.26	2.843 ± 0.0003	-	-	-	-
V* TZ Pic	7.74	1.05	4673	1.34	13.839 ± 0.008	10^{-5}	12.50 ± 0.35	0.78	$< 10^{-15}$
V* UU Lep	6.94	1.11	4674	1.88	-	-	5.36 ± 0.21	0.31	$< 10^{-15}$
V* UV For ★	8.06	0.99	4814	0.97	66.447 ± 0.135	10^{-11}	8.54 ± 0.23	0.71	$< 10^{-15}$
V* UX Col	10.59	1.03	5076	-	0.970 ± 0.00002	$< 10^{-15}$	11.35 ± 1.20	0.33	$< 10^{-15}$
V* UX For	8.06	0.72	5281	-0.04	22.035 ± 0.016	10^{-7}	8.93 ± 0.31	0.42	$< 10^{-15}$
V* UY For ★	8.25	1.15	4541	1.98	16.144 ± 0.010	10^{-9}	8.51 ± 0.42	0.20	$< 10^{-15}$
V* V1017 Sco ★	7.99	1.16	4896	2.06	66.356 ± 0.152	$< 10^{-15}$	13.42 ± 0.23	1.17	$< 10^{-15}$
V* V1257 Cen ★	11.68	1.01	4308	-0.48	2.761 ± 0.0003	$< 10^{-15}$	18.14 ± 0.91	1.05	$< 10^{-15}$
V* V1265 Cen	11.01	-	4361	0.86	3.533 ± 0.0001	-	-	-	-
V* V1335 Cen	10.06	0.59	5863	0.26	1.695 ± 0.0001	10^{-11}	7.35 ± 0.16	0.20	$< 10^{-15}$
V* V1355 Ori ★	9.19	0.86	4856	0.62	3.863 ± 0.0002	$< 10^{-15}$	10.08 ± 1.30	0.66	$< 10^{-15}$
V* V2253 Oph ★	8.49	1.17	4767	1.66	21.544 ± 0.009	$< 10^{-15}$	19.37 ± 2.27	0.50	$< 10^{-15}$
V* V344 Pup	6.89	1.06	4778	1.45	11.757 ± 0.001	-	-	-	-
V* V354 Lib ★	11.34	1.23	4439	0.37	5.623 ± 0.0004	$< 10^{-15}$	13.30 ± 1.36	1.19	$< 10^{-15}$

Table 1. (continued)

ID	<i>V</i>	<i>B – V</i>	<i>T</i> _{eff} [K]	<i>log L</i> [<i>L</i> _⊙]	<i>P</i> _{rot} [d]	FAP (<i>P</i> _{rot})	<i>P</i> _{cyc} [yr]	<i>A</i> _{cyc} [%]	FAP (<i>P</i> _{cyc})
V* V356 Pup \ddagger	8.21	1.21	4445	2.12	37.306	-	4.20 ± 0.08	0.30	10^{-13}
V* V4091 Sgr	8.45	1.16	4527	1.56	16.932 ± 0.011	-	-	-	-
V* V4138 Sgr \star	6.74	1.02	4713	1.18	61.933 ± 0.067	$< 10^{-15}$	5.35 ± 0.09	0.92	$< 10^{-15}$
V* V4139 Sgr	8.45	1.17	4363	1.66	44.828 ± 0.018	-	-	-	-
V* V414 Hya \star	8.90	1.06	4586	1.39	18.750 ± 0.004	$< 10^{-15}$	5.51 ± 0.31	0.41	10^{-12}
V* V592 Pup	7.86	0.61	6023	0.45	1.967 ± 0.0001	-	-	-	-
V* V764 Cen	8.91	1.37	4541	1.52	22.519 ± 0.019	$< 10^{-15}$	12.43 ± 0.53	1.25	$< 10^{-15}$
V* V789 Mon	9.39	0.96	4648	-0.50	1.401 ± 0.0001	$< 10^{-15}$	13.47 ± 1.65	0.53	$< 10^{-15}$
V* V829 Cen	7.84	0.93	4614	1.32	11.707 ± 0.003	$< 10^{-15}$	10.30 ± 0.30	0.41	$< 10^{-15}$
V* V841 Cen \star	8.57	1.06	4588	0.60	5.997 ± 0.001	$< 10^{-15}$	4.32 ± 0.52	0.23	10^{-4}
V* V851 Cen	7.80	0.94	4700	0.74	12.225 ± 0.007	10^{-9}	13.60 ± 0.17	1.33	$< 10^{-15}$
V* V858 Cen	10.45	0.88	4939	-0.41	1.037 ± 0.00002	$< 10^{-15}$	20.05 ± 0.96	0.91	$< 10^{-15}$
V* V965 Sco \star	8.57	0.95	4707	1.81	30.544 ± 0.025	$< 10^{-15}$	4.51 ± 0.04	0.43	$< 10^{-15}$
V* V991 Sco \ddagger	9.69	0.68	5498	0.28	3.300	-	5.97 ± 0.17	0.23	$< 10^{-15}$
V* VV Mon \ddagger	9.40	0.81	4978	1.05	6.051	-	-	-	-
V* VX Pyx	6.37	0.95	5046	1.77	-	-	9.43 ± 0.48	0.33	$< 10^{-15}$
V* YZ Men \star	7.77	1.08	4594	1.50	19.216 ± 0.006	$< 10^{-15}$	16.99 ± 2.38	1.31	$< 10^{-15}$